Structural Color Modulation by Controllable Fabricating of Two-Dimensional Metal Nanoarrays

Xiu Li, Lingzhi Liu, Yuchen Ren, Jiong Liang, and Min Huang

***Abstract*—The structural coloration of two-dimensional photonic crystals has always been a hot topic in recent research. However, how to control the arrangement of nano particles in two-dimensional periodic structure so as to produce specific hue of structural colors with stable physical properties, have become key research content. In order to overcome this drawback, a method of utilizing plasma etching treatment to create structural color modulation on two-dimensional colloidal crystal surfaces by changing the etching power has been proposed. Colors as orange red, yellow, green and blue are obtained with different plasma etching power on planar hexagonal packed structure. The effects of plasma etching power and sizes of PS particles on the optical properties are studied. As a result, the color of samples distributed counterclockwise around white point with increasing the plasma etching power on the a∗ - b∗ plane, and changed from orange to blue. Moreover, the diffraction spectrum is also experimentally investigated, and exceed the sRGB gamut boundary. This research can be used in the applications of green printing, anti-counterfeiting and other related fields with low cost.**

***Index Terms*—Plasma etching power, plasma surface modification, structural color, two-dimensional photonic crystal.**

I. Introduction

STRUCTURAL color [1], [2] is a common coloration in nature which can be found in butterfly wings, beetles, peacock feathers, and pearls, etc.. Recently, structural colors are attracting much attention due to high brightness, strong stability, and low environmental burden. The formation of this kind color does not require chemical dyes or pigments, but the interaction between light and periodic nanostructures such as thin-film interference, diffraction grating effect, photonic crystals and light scattering that can produce vivid colors covering the entire visible light. [3], [4] Therefore, inspired by this, the regulation of structural color also has a very promising development prospect in the fields of color printing [5] and anti-counterfeiting [6]. Joo Hwan Ko et al. presented a flexible, large-area covert polarization display by using ultrathin lossy nanocolumns with wide color deposited on a metal film without structurally sophisticated fabrication processes [7]. Young Jin Yoo et al. demonstrated ultra-thin, fine-tunable optical coatings with enhanced color purity based on highly absorbent porous media on metal substrate, which could be widely used as an effective method to enhance the optical characteristics needed in applications such as colorizing metals and thin-film absorbers [8].

Structural color can be produced by various methods, including additive manufacturing [9], [10], lithography [11], laser direct writing [12] and colloidal assembly [13], etc.. Among of them, the two dimensional (2D) photonic crystals (PCs) fabricated by self-assembly strategies such as magnetic assembly, microfluidics, spray coating, and printing, etc., have attracted much attention on account of the simple preparing procedure, low cost and high production efficiency. Honghu Zhang et al. [14] used the regular network-structured arrays which were fabricated by monolayer colloidal template-induced solution-dipping strategy, which were used as the second templates to prepare periodic nanoparticle arrays by further sputtering deposition. The periodic nanostructure array exhibited highly stable and sensitive surface enhanced Raman scattering (SERS) performance [15]. By controlling the deposition time, the nano gap between two adjacent spherical nanoparticles can be well adjusted. Men Dandan et al. Zhu Xiaolong et al. [16] studied the methods of plasma nanostructures and colors generated by metasurfaces. They showed a method of color printing using laser post writing on the surface of nano imprinted plasma elements. Laser pulses cause transient local heating, leading to the melting and remodeling of imprinted nanostructures. Based on the energy density of laser pulses, different surface morphologies supporting different plasma resonances can be generated, resulting in different color appearances. Li Fenghang et al. [17] presented a facile and low-cost method to prepare periodic Au@metal–organic framework (MOF) (MIL-100(Fe)) nanoparticle arrays. A monolayer colloidal crystal was prepared using a gas-liquid interface self-assembly process, and the Au film with a certain thickness was deposited on this PS colloidal monolayer using magnetron sputtering deposition to prepare Au coatings on the PS spheres. The periodic Au nanosphere array was obtained on the quartz substrates by annealing the colloidal monolayer with Au coating in a furnace at 900°C for 2h. FABIO A. KRAFT et al. [18] suppressed the mechanochromatic effect of flexible photonic crystal slabs (PCS) via the formation of photonic crystal cells of rigid waveguiding layers under external stress. They manufactured stable photonic crystal plates (sPCS) based on nanoimprinting technology and studied three different types of PCS - two types of stable PCS (sPCS), known as Type I and Type II. The sPCS concept uses a highly flexible TiO_2 nanoparticle layer as high-index waveguide layer that deforms with the substrate and thus exhibits mechanochromism. Julia

Manuscript received 26 October 2023; revised 14 December 2023; accepted 23 December 2023. Date of publication 3 January 2024; date of current version 24 January 2024. This work was supported by College's Scientific Research Project under Grants BIGC Ec202003, BIGC Eb202102, and BIGC Ec202302. *(Corresponding author: Min Huang.)*

The authors are with the Beijing Institute of Graphic Communication, Beijing 102600, China (e-mail: huangmin@bigc.edu.cn).

Digital Object Identifier 10.1109/JPHOT.2023.3347569

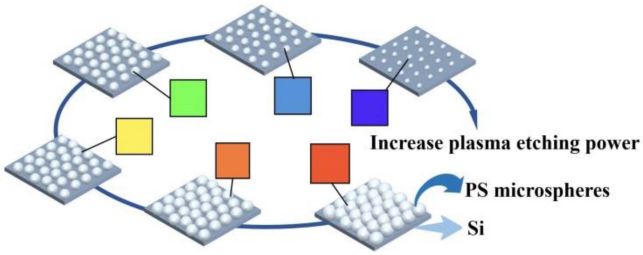

Fig. 1. Schematic illustration of the shape of the PS particle variation with different plasma etching power.

Kredel et al. [19] studied the combination of soft core and soft shell particles with only adjustable hard intermediate layers for the preparation of compressed responsive photonic crystals. By combining high fluorinated shell materials and aromatic copolymer as core materials, the refractive index comparison between the core and shell materials is increased. Opal films can be prepared by melt shear texturing under moderate pressure and temperature. By adding UV crosslinking agent and studying its UV crosslinking ability, the pattern inside the prepared opal film can be fine tuned or fixed after the space limiting pressure is applied, thus changing the reflection color of opal film locally.

In this article, we mainly explored a method of utilizing plasma etching treatment to create structural color modulation on two-dimensional periodic substrates by changing the etching power. [20] The two-dimensional (2D) close-packed template were fabricated via air-water self-assembly method [21], and then were etched by oxygen plasma etching method. The particle size of PS microspheres was controlled by plasma treatment power, which will affect the optical properties of the whole substrate. It indicated that the higher the plasma etching power is, the bigger etching rate will be, and the colloidal particle size will be smaller.

II. Experiment

The fabrication process of monolayer polystyrene (PS) microsphere [22] arrays with tunable periodic lengths is shown in Fig. 1. First, the two-dimensional (2D) close-packed colloidal crystals with a particle size of 300 nm are fabricated via air-water self-assembly method, and then transferred to the silicon substrate to form a periodic template. Then the prepared 2D periodic PS microsphere substrate array is etched by oxygen plasma treatment to change the particle size of the microsphere. The etching rate depends on several working conditions such as power, gas flow, etching time, etc.. In this experiment, the plasma treatment time is set to 5 min and the O_2 flow rate is 30 SCCM, and the PS particle size can be controlled by changing the power of plasma etching. Theoretically, when the etching time and oxygen flow are constant, the higher the plasma etching power is, the bigger etching rate will be. Accordingly, the colloidal particle size will be smaller. In response to this prediction, five different plasma etching powers (15 W, 30 W, 60 W, 90 W, and 120 W) are set in this experiment to explore the relationship between the microstructure of PS particle arrays and the parameters of plasma etching.

In addition, in order to further investigate the color turning mechanism of samples before and after plasma etching procedure with different power, the Au thin film is deposited on the surface of the sample mentioned above by magnetron sputtering [23]. The thickness of the Au film is controlled by adjusting the sputtering current and time, which is fixed at 15 mA and 80 s, respectively.

III. Results and Discussion

A. Characterization of 2D Non-Close-Packed Colloidal Crystal Arrays

Fig. 2 demonstrated the characterization of 2D colloidal crystal arrays controlled by plasma etching process before and after deposition with Au thin film. Fig. 2(a)–(f) showed the SEM images of the PS colloidal monolayers with different plasma etching power. It can be seen that the PS microspheres showed planar hexagonal densely packed structure without obvious defects before plasma etching (Fig. 2(a)). As increasing the plasma etching power from 15W to 90W (Fig. 2(b)–(e)), the diameter of PS nanoparticles decreased gradually to form non-densely arranged periodic arrays while the periodic length is almost the same as that of PS template mentioned in Fig. 2(a). Fig. 2(b) illustrated the micro morphology of the sample under 15W plasma treating. Compared with the original template, the diameter of PS microspheres decreased slightly with the distribution between 290 nm to 300 nm, showing a hexagonal packed structure. Keep up increasing the plasma etching power, the particle size can be reduced further, and distributed between 270 nm to 280 nm, 250 nm to 270 nm, and 230 nm to 240 nm under the treating power of 30 W, 60 W and 90 W, respectively, while the periodic length almost remain the same. It can also been observed that the particle size of PS microsphere decreased obviously under 90 W plasma treating. Moreover, the arrangement of PS microsphere with non-densely planar hexagonal packed structure was quite homogeneous and defect-free in a certain domain. When the plasma etching power reached to 120 W (Fig. 2(f)), the PS microspheres were etched into smaller particles with distribution from 170 nm to 200 nm. At the same time, the microspheres were etched into irregular spherical particles, and the periodicity was even destroyed to some degree. Fig. 2(m)–(r) depicted the particle size distribution of samples treated with different plasma etching power. The size distribution of the nanospheres was narrow and the central particle sizes were 328 nm, 300 nm, 290 nm, 280 nm, 236 nm, 185 nm, respectively.

Fig. 2(g)–(l) indicated the SEM images of the samples obtained from Fig. 2(a)–(f) with deposition of Au thin film by magnetron sputtering method, and the thickness of the Au film can be characterized by sputtering time. The thickness of the coating is determined by the following formula based on empirical method

$$d = KIVT \tag{1}$$

According to (1), d represents the coating thickness (in Å); K is a constant, related to the material used for sputtering the target and the gas filled in the chamber; I is the current (in mA), V is the applied voltage (in KV), T is the sputtering time (in

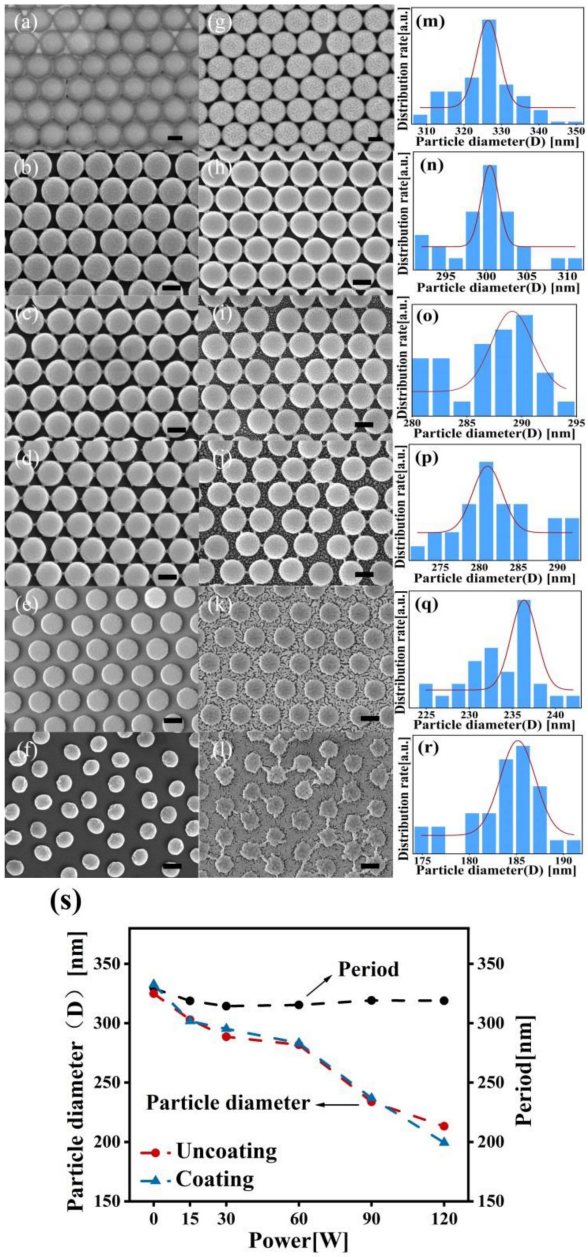

Fig. 2. (a)–(l) are the SEM images of the PS colloidal monolayers with the plasma etching power changing from 0–120 W before and after sputtering with Au; (m)–(r) are the particle size distribution of samples treated with different plasma etching power; (s) is the average particle size and periodic length of microsphere changing with plasma etching power before and after sputtering with Au. The scale bar is 200 nm.

seconds). The sputtering target material used in this experiment is Au, and the gas introduced is air, so the K value is 0.07, the sputtering current is 15 mA, the working voltage is 0.6 KV, which was fixed at 80s in the experiment for about 50.4Å Au thickness. As shown in Fig. 2(g), the particle size of the coated microspheres was between 310 nm and 330 nm, and the microspheres were arranged in a close-packed hexagonal lattice structure. That is to say, the monolayer periodic arrays maintained good consistency after sputtering treatment for 80 s. As the plasma etching power increased (Fig. 2(h)–(l)), the Au nanoparticles were uniformly deposited on the surface of the PS microspheres, and the particle sizes increased slightly. Accordingly, the surface became rougher under high etching power, especially under the etching power of 90 W and 120 W. This is because as the plasma power increases, the particle size of the microspheres is etched to be very small. After sputtering with Au, the particles will be unevenly distributed on the surface of the microspheres, which will cause the periodicity of two-dimensional photonic crystals to be disrupted.

Fig. 2(s) displayed the curve of the average particle size and periodic length of microsphere changing with plasma etching power before and after sputtering with Au. It can be seen that the particle size of PS microspheres gradually decreased with the increase of plasma etching power, while the periodic length did not change significantly. The average size of the nano particles is 301 nm, 285 nm, 277 nm, 233 nm and 182 nm as the plasma etching power increased from 15 W to 120 W before sputtering with Au, while the diameters increased slightly after Au coating treatment. In addition, the periodic length was almost the same as that of the PS template, which was around 300 nm.

B. Optical Properties of 2D Non-Close-Packed Colloidal Crystal Arrays

In the experiment, the reflectance spectra of as-prepared samples under different O_2 plasma etching power before and after Au sputtering had been invesgated with specular reflection of 20°, as shown in Fig. 3(a) and (b), in which we can see the colors were created by the absorption of light at a certain wavelength range corresponding to the valleys in the reflectance. In Fig. 3(a), it exhibited that the reflective color was turned in the visible range deriving from the periodic structure of the PS nanoparticles array upon increasing the plasma etching power. With a gradual increase in the plasma etching power from 0 to 120 W, the dips in reflectance were observed to progressively blue shift from $\lambda = 700$ nm to 380 nm, which was due to the phase change of reflection coefficients varies with particle size of PS [8]. The sample was mainly orange-red with low saturation before plasma etching process, and the whole surfaces of the substrates presented pale and dim structural colors in orange, yellow-green, green and blue due to the different plasma etching power of 10, 15, 30, 60, 75 and 90 W, respectively, which can result in the specular color observed in the inset of Fig. 3(a). When the processing power was 120 W, the reflectance spectrum curve only presented a very small reflection peak in short wavelength, so there wasn't any obvious color for the sample. Fig. 3(b) exhibited the reflectance spectrum of the samples after coated with Au for 80 s. It can be observed that compared with Fig. 3(a), the color saturation was significantly increased due to the absorption of the scattered light by the metal nanoparticles [24], [25], [26], [27], [28] and the resonance enhancement of periodic metal nanolayer. The central wavelength of the absorption had a significant shift from 500 nm to around 350 nm in the visible range with the plasma treatment power changing from 0 W to 120 W, and thus a large color space can be covered. Additionally,

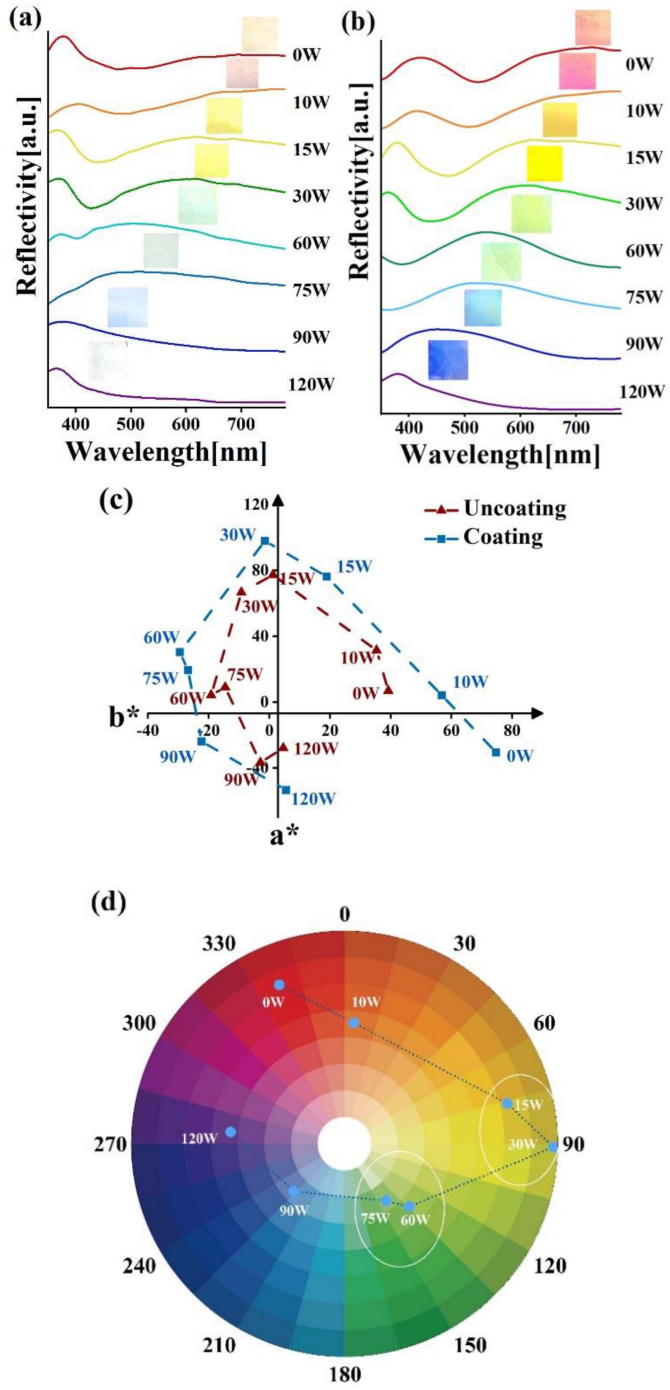

Fig. 3. Reflectance spectra and optical photos of samples treated with different plasma etching power before (a) and after (b) sputtering with Au; (c) is a ∗ - b ∗ color coordinates in CIELab uniform color space; (d) the relationship between the particle size and the corresponding structural color.

the optical images shown in the inset of Fig. 3(b) were bright and vivid and changed from orange red to yellow, then to green and finally to blue with increasing the plasma processing power.

Fig. 3(c) and Table I demonstrated the chromaticity index L∗, a∗, b∗ in the CIELAB color space [29] for the samplas treated by different plasma etching power before and after sputtering

TABLE I
CALCULATED VALUE OF CIELAB

	Uncoating			Coating with 80s		
	L	a*	b*	L	a*	b*
0W	51.46	39.22	6.83	57.68	74.69	-30.57
10W	64.85	35.35	31.44	58.83	56.82	4.16
15W	87.24	1.17	77.25	83.45	18.89	76.29
30W	93.93	-9.22	66.68	90.34	-1.46	97.94
60W	94.18	-19.16	4.27	95.08	-29.47	30.34
75W	96.74	-14.55	8.96	95.58	-26.80	19.41
90W	62.05	-2.94	-36.80	84.07	-22.35	-23.93
120W	49.10	4.60	-27.90	45.42	5.50	-53.46

with Au thin film. The chromaticity index a∗ and b∗ were first studied in order to explore the color changing law of the 2D colloidal crystal arrays controlled by plasma etching process. In the a∗-b∗ plane (see Fig. 3(c)), samples sputtering with Au (blue squares) distributed counterclockwise around white point with increasing the plasma etching power on the plane, and the color of the samples changed from orange to blue-purple; samples without coating Au (red triangles) distributed inside the big loop formed by blue squares and the red triangles were closer to the white spot than the blue squares. It indicated that they were essentially different and the sample sputtered by Au thin film had a wider distribution area in a∗-b∗ diagram, corresponding to a higher color saturation. In Fig. 3(d), it can be clearly seen that the sample presented orange-red before O_2 plasma etching treatment, and it turned to be orange under etching power of 10 W. When the power reached 15 W–30 W and 60 W–75 W, the color remained yellow-green and green, respectively, then as the power raised to 90 W, the sample presented biue, and finally gradually approached violet with etching power of 120 W.

Fig. 4 presented the diffraction spectrum and the a ∗ - b ∗ chromaticity coordinates in CIELAB color space of samples treated with different plasma etching power at detection angles of 40°, 45° and 50°, respectively. From Fig. 4(a) and (b), it can be seen that the peak position of the diffraction spectrum before and after coated with Au moved to the long wavelength with the increase of the detection angle. Overall, the peaks of the diffraction spectrum distributed in the short wavelength, and had no obvious change after sputtering with Au as well. With the increase of plasma etching power, the diffraction peak position of the samples had no obvious change while the saturation changed obviously. As can be seen in Fig. 4(c) and (d), in CIELAB uniform color space, the color coordinates of samples distributed in the fourth quadrant of a∗-b∗ plane, and Table II showed the CIELAB values calculated from diffraction spectrum by comparing the equal Munsell hue and equal Munsell chromaticity tracks on the CIELAB uniform color space a∗-b∗ plane, we can see that the diffraction of the sample at this time is purple. As the diffraction angle and the plasma etching power increaseed, the chromaticity coordinate distribution of the sample was farther away from the white spot and showed an approximate linear distribution, which indicating the samples contained the

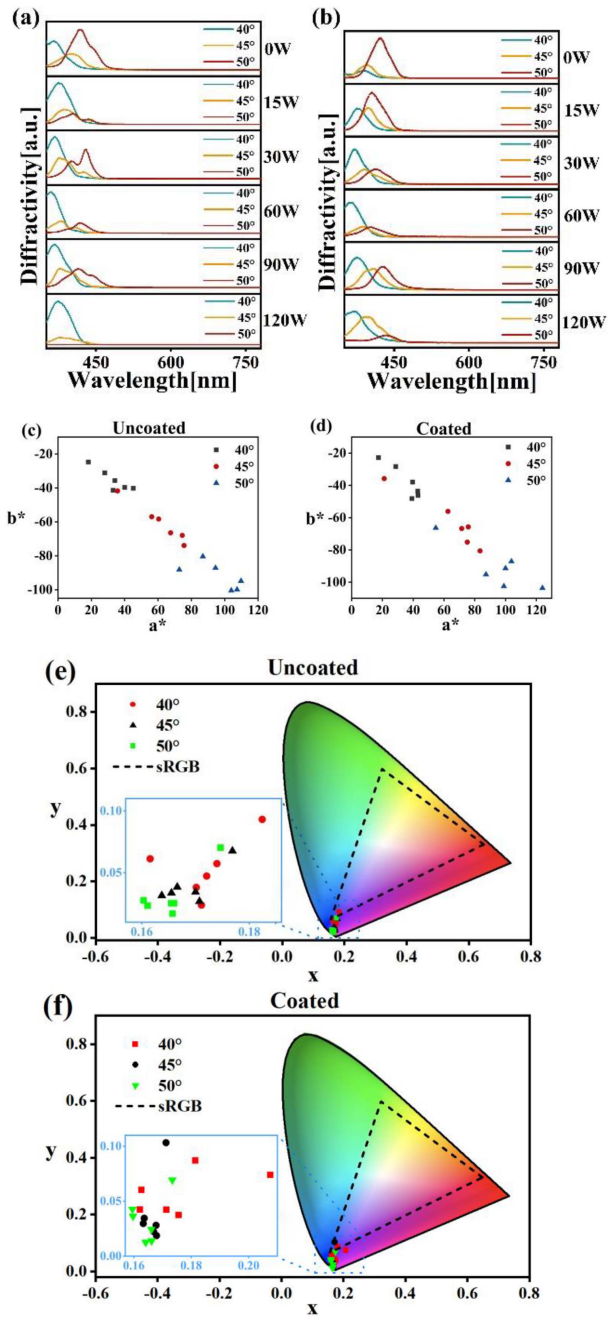

Fig. 4. Diffraction spectrum of samples at different diffraction angles before (a) and after (b) sputtering with Au; (c) The coordinates of the diffraction color of the uncoated sample in the CIELAB uniform color space a∗-b∗ plane; (d) The coordinates of the diffraction color of the coated sample in the CIELAB uniform color space a∗-b∗ plane; (e) The x-y chromaticity coordinates of uncoated samples in the CIExyz color space at different diffraction angles. (f) The x-y chromaticity coordinates of the coated samples in the CIExyz color space at different diffraction angles.

hue invariant and the saturation increased. Subsequently, the spectrum data were also drawn in the standard CIE1931 chromaticity diagram, as shown in Fig. 4(e) and (f). The path of the color variations further demonstrated that the color changed slightly with plasma etching power varying from 0 to 120 W under different detecting angles, while exceed the sRGB color space.

TABLE II
CALCULATED VALUE OF LA∗B∗ OF SAMPLE UNDER DIFFRACTION SPECTRUM

		Uncoating			Coating 80s		
		L	a*	b*	L	a*	b*
0	40°	2.94	33.07	-41.36	0.05	42.92	-43.54
	45°	7.02	75.58	-73.93	-1.33	62.56	-56.15
	50°	10.65	107.37	-99.92	4.63	123.93	-103.71
15W	40°	-2.24	40.01	-39.66	-2.91	39.59	-37.94
	45°	5.47	67.53	-66.48	-0.25	75.77	-65.77
	50°	6.40	86.87	-80.39	2.17	103.80	-87.18
30W	40°	-2.21	28.05	-31.10	-0.70	28.64	-28.33
	45°	3.14	60.36	-58.35	3.62	71.50	-66.77
	50°	5.69	109.75	-94.85	8.95	99.95	-91.46
60W	40°	-0.51	18.20	-24.73	-2.47	17.43	-22.76
	45°	4.65	35.73	-41.77	8.09	21.18	-35.80
	50°	8.27	94.44	-87.15	17.28	54.66	-66.40
90W	40°	-1.98	34.09	-35.64	0.96	43.10	-46.24
	45°	3.82	56.25	-57.01	8.33	83.42	-80.65
	50°	13.18	103.90	-100.47	18.96	87.27	-95.29
120W	40°	-5.11	45.14	-40.21	5.86	39.12	-48.16
	45°	3.55	74.54	-67.98	8.59	75.13	-75.21
	50°	28.68	72.73	-88.19	18.39	98.87	-102.59

IV. CONCLUSION

In summary, a method of utilizing plasma etching technology to realize modulation of structural colors on two-dimensional colloidal crystal surfaces by changing the etching power had been proposed in this article. Colors as orange red, yellow, green and blue were experimentally obtained with different plasma etching power from low to high under a certen etching time. The two-dimensional (2D) close-packed colloidal crystals with a particle size of 300 nm were fabricated via air-water self-assembly method, then the prepared template was etched by oxygen plasma treatment to change the particle size of the microspheres. As increasing the plasma etching power, the periodicity of PS microspheres remains unchanged and still distributed in a planar hexagonal densely packed structure, while the the particle size was smaller in center. Meanwhile, we also investigated the influence of PS particle sizes on optical performance of samples, wherein along with a gradual increase of the plasma etching power from 0 to 120 W, there was an obvious blue-shift for the two reflection peak positions. This research provides possibilities for the experimental research and applications of controllable structural color.

REFERENCES

[1] P. M. Liu et al., "Self- assembled colloidal arrays for structural color," *Nanoscale Adv.*, vol. 1, no. 5, pp. 1672–1685, 2019.
[2] X. Hou et al., "Recent progress in responsive structural color," *J. Phys. Chem. Lett.*, vol. 13, no. 13, pp. 2885–2900, 2022.
[3] Z. Zhang et al., "Structural color materials from natural polymers," *Adv. Mater. Technol.*, vol. 6, no. 11, 2021, Art. no. 2100296.
[4] K. Zhu et al., "Recent advances in photonic crystal with unique structural colors: A review," *J. Mater. Sci. Technol.*, vol. 141, pp. 78–99, 2023.
[5] S. Choi et al., "Structural color printing via polymer-assisted photochemical deposition," *Light-Sci. Appl.*, vol. 11, no. 1, 2022, Art. no. 84.
[6] C. Ji et al., "Quadruple anti-counterfeiting retroreflective structural color films," *Adv. Opt. Mater.*, vol. 10, no. 5, 2022, Art. no. 2102383.
[7] J. H. Ko et al., "Flexible, large-area covert polarization display based on ultrathin lossy nanocolumns on a metal film," *Adv. Funct. Mater.*, vol. 30, no. 11, 2020, Art. no. 1908592.

[8] Y. J. Yoo et al., "Ultra-thin films with highly absorbent porous media fine-tunable for coloration and enhanced color purity," *Nanoscale*, vol. 9, no. 9, pp. 2986–2991, 2017.
[9] B. M. Boyle et al., "Structural color for additive manufacturing: 3D-printed photonic crystals from block copolymers," *ACS Nano*, vol. 11, no. 3, pp. 3052–3058, 2017.
[10] B. A. Rorem et al., "Integrating structural colors with additive manufacturing using atomic layer deposition," *ACS Appl. Mater. Interfaces*, vol. 14, no. 27, pp. 31099–31108, 2022.
[11] C. L. Luo et al., "Large-scale structural color on transparent plexiglass by nanosphere lithography combined with reactive-ion etching," *Opt. Mater.*, vol. 135, 2023, Art. no. 113273.
[12] R. Liu et al., "Laser interference lithography-A method for the fabrication of controlled periodic structures," *Nanomaterials*, vol. 13, no. 12, 2023, Art. no. 1818.
[13] A. T. L. Tan et al., "Direct-write freeform colloidal assembly," *Adv. Mater.*, vol. 30, no. 44, 2018, Art. no. 1803620.
[14] H. Zhang et al., "Spherical nanoparticle arrays with tunable nanogaps and their hydrophobicity enhanced rapid SERS detection by localized concentration of droplet evaporation," *Adv. Mater. Interfaces*, vol. 2, no. 9, 2015, Art. no. 1500031.
[15] D. Liu et al., "Air-liquid interfacial self-assembly of two-dimensional periodic nanostructured arrays," *Chemnanomat*, vol. 5, no. 11, pp. 1338–1360, 2019.
[16] X. Zhu et al., "Plasmonic colour laser printing," *Nature Nanotechnol.*, vol. 11, no. 4, pp. 325–334, 2016.
[17] L. Hang et al., "Functionalized periodic Au@MOFs nanoparticle arrays as biosensors for dual-channel detection through the complementary effect of SPR and diffraction peaks," *Nano Res.*, vol. 10, no. 7, pp. 2257–2270, 2017.
[18] F. A. Kraft et al., "Suppressing the mechanochromism of flexible photonic crystals," *Opt. Exp.*, vol. 31, no. 4, pp. 6281–6295, 2023.
[19] J. Kredel and M. Gallei, "Compression-responsive photonic crystals based on fluorine-containing polymers," *Polymers*, vol. 11, no. 12, 2019, Art. no. 2114.
[20] Y. Chen et al., "A facile, low-cost plasma etching method for achieving size controlled non-close-packed monolayer arrays of polystyrene nanospheres," *Nanomaterials*, vol. 9, no. 4, 2019, Art. no. 605.
[21] X. Ye et al., "Monolayer colloidal crystals by modified air-water interface self-assembly approach," *Nanomaterials*, vol. 7, no. 10, 2017, Art. no. 291.
[22] G. Rosetta et al., "Chromaticity of structural color in polymer thin film photonic crystals," *Opt. Exp.*, vol. 28, no. 24, pp. 36219–36228, 2020.
[23] J. T. Gudmundsson, "Physics and technology of magnetron sputtering discharges," *Plasma Sources Sci. Technol.*, vol. 29, no. 11, 2020, Art. no. 113001.
[24] X. He et al., "Multi-mode structural-color anti-counterfeiting labels based on physically unclonable amorphous photonic structures with convenient artificial intelligence authentication," *J. Mater. Chem. C*, vol. 7, no. 45, pp. 14069–14074, 2019.
[25] Y. Li et al., "Inkjet printed physically-unclonable structural-color anticounterfeiting labels with convenient artificial intelligence authentication," *Adv. Mater. Interfaces*, vol. 8, no. 21, 2021, Art. no. 2101281.
[26] J. Wang et al., "Wearable nanocomposite hydrogel temperature sensor based on thermally-switchable and mechanical-deformation-insensitive structural colors," *Chem. Eng. J.*, vol. 476, 2023, Art. no. 146602.
[27] J. Zhou et al., "Self-healable organogel nanocomposite with angle-independent structural colors," *Angewandte Chemie-Int. Ed.*, vol. 56, no. 35, pp. 10462–10466, 2017.
[28] Y. Zhang et al., "Highly brilliant noniridescent structural colors enabled by graphene nanosheets containing graphene quantum dots," *Adv. Funct. Mater.*, vol. 28, no. 29, 2018, Art. no. 1802585.
[29] B. Hill, T. Roger, and F. W. Vorhagen, "Comparative analysis of the quantization of color spaces on the basis of the CIELAB color-difference formula," *ACM Trans. Graph.*, vol. 16, no. 2, pp. 109–154, Apr. 1997.